Silk fibroin scaffolds with inverse opal structure for bone tissue engineering

Marianne R. Sommer,[1] Jolanda R. Vetsch,[2] Jessica Leemann,[1] Ralph Müller,[2] André R. Studart,[1] Sandra Hofmann[2,3,4]

[1]Department of Materials, Complex Materials, ETH Zurich, 8093 Zurich, Switzerland
[2]Department of Health Science and Technology, Institute for Biomechanics, ETH Zurich, 8093 Zurich, Switzerland
[3]Department of Biomedical Engineering, Eindhoven University of Technology, 5600MB Eindhoven, the Netherlands
[4]Institute for Complex Molecular Systems, Eindhoven University of Technology, 5600MB Eindhoven, the Netherlands

Abstract: How scaffold porosity, pore diameter and geometry influence cellular behavior is-although heavily researched - merely understood, especially in 3D. This is mainly caused by a lack of suitable, reproducible scaffold fabrication methods, with processes such as gas foaming, lyophilization or particulate leaching still being the standard. Here we propose a method to generate highly porous silk fibroin scaffolds with monodisperse spherical pores, namely inverse opals, and study their effect on cell behavior. These silk fibroin inverse opal scaffolds were compared to salt-leached silk fibroin scaffolds in terms of human mesenchymal stem cell response upon osteogenic differentiation signals. While cell number remained similar on both scaffold types, extracellular matrix mineralization nearly doubled on the newly developed scaffolds, suggesting a positive effect on cell differentiation. By using the very same material with comparable average pore diameters, this increase in mineral content can be attributed to either the differences in pore diameter distribution or the pore geometry. Although the exact mechanisms leading to enhanced mineralization in inverse opals are not yet fully understood, our results indicate that control over pore geometry alone can have a major impact on the bioactivity of a scaffold toward stem cell differentiation into bone tissue. © 2016 The Authors Journal of Biomedical Materials Research Part B: Applied Biomaterials Published by Wiley Periodicals, Inc. J Biomed Mater Res Part B: Appl Biomater, 105B: 2074–2084, 2017.

Key Words: bone tissue engineering, human mesenchymal stem cells, scaffold, silk fibroin, porous structure

How to cite this article: Sommer MR, Vetsch JR, Leemann J, Müller R, Studart AR, Hofmann S. 2017. Silk fibroin scaffolds with inverse opal structure for bone tissue engineering. J Biomed Mater Res Part B 2017:105B:2074–2084.

INTRODUCTION

The increasing need for bone replacement surgeries in patients suffering from osteoporosis and fractured or diseased musculoskeletal tissue has strongly motivated the development of new artificial bone substitutes.[1–4] These artificial materials are typically porous scaffolds consisting of natural and/or synthetic materials that are placed in the damaged area to promote fast and full repair of the skeletal tissue. Integration between host tissue and implanted scaffold requires the attachment, in-growth and extracellular matrix production of cells into the porous structure. Recent research efforts have focused on the development of porous scaffolds that could provide physical and chemical cues to accelerate the bone regeneration process. Physical parameters such as pore architecture, elastic modulus and topography have been shown to be influential properties of scaffolds affecting not only cell attachment but also subsequent tissue regeneration. Pore sizes larger than 300 μm have been reported to be beneficial *in vivo* and a minimal necessary pore size of 100 μm has been suggested.[5] Pore shape has been shown to control the mode of tissue in-growth through local tissue curvature minimization.[6] Also, Engler et al. observed distinct gene expression patterns related to specific differentiation pathways when human mesenchymal stem cells (hMSC) were cultured on 2D substrates with elastic moduli similar to those of various tissues.[7] Similarly, Kumar et al. observed increased osteocalcin expression on scaffolds with a rougher microstructure.[8] In addition to such physical parameters, the chemical composition of the scaffold also plays a crucial role in their ability to promote bone regeneration.[9]

A wide range of materials has been exploited to create scaffolds for tissue engineering. Scaffolds made of silk fibroin (SF) have been shown to be highly suitable for engineering of bone[10–12] owing to their crystallinity and therefore relatively high stiffness and slow degradation compared to other proteinaceous materials.[13] Moreover, the structure of SF scaffolds was found to be an important factor in tissue engineering studies.[1,14] In our own studies, we found that the pore size range of SF scaffolds influenced the morphology of the regenerated bone initially, even if after 5 weeks in culture those differences disappeared.[1] So far, such scaffolds could be produced by porogen leaching, gas foaming or lyophilisation.[1,15] Because it can lead to relatively narrow pore size distributions, the porogen leaching method using sieved salt particles or paraffin globules as templates has been particularly attractive.[1,3] In this sacrificial template approach, porogen particles are first assembled, infiltrated with the biocompatible/bioresorbable material of interest and eventually removed by dissolution or pyrolysis to result in a porous scaffold. A drawback of this route is that the irregular and non-spherical nature of the templating salt granules often used in this technique generates ill-defined packing geometries and therefore provides a rather heterogeneous local environment to the cells.

One possible approach toward more homogeneously structured scaffold fabrication is the use of monodisperse and spherical pore templating microparticles that can be assembled into a crystalline lattice before infiltration. Dissolution of the template creates pores of the same diameter that are ordered in closely packed arrangements throughout the scaffold, leading to so-called inverse opals (IO).[16] Besides monodispersity, such porogen templating particles have to meet several other requirements. Solubility in a solvent, which the scaffold material is resilient to, ensures that the templates can be leached from the scaffold after microparticle assembly and infiltration. Compatibility with the infiltration solution is necessary in order prevent damage or alteration of the porogen particles that could eventually also impact the resulting pore geometry. Also, the resulting scaffold material must not contain any cytotoxic residues from the production process. Finally, tunability of the porogen particle diameter in the pore range of interest to tissue engineering, namely between 100 and 500 μm,[5] is desirable since it allows for studying the influence of pore diameter on cell response.

Templating microparticles that are extremely uniform in diameter can be produced using droplet-based microfluidics. Choi et al. have prepared poly(lactic acid-co-glycolic acid) (PLGA) inverse opal scaffolds using gelatin spheres made by microfluidics as templates.[17,18] Commercially available poly(methyl methacrylate) (PMMA) or polystyrene latex beads have also been used to create PLGA or poly(hydroxyethyl methacrylate) (pHEMA) inverse opals.[19,20] Such scaffolds made with PLGA have been shown to facilitate a more homogeneous cell seeding as compared to disordered structures of equivalent pore diameter. The faster diffusion of macromolecules observed by Choi et al. has possibly led to a less steep gradient in medium composition from the scaffold's edge to the center.[18] However, the relatively fast degradation as well as acidic side products limit the use of PLGA as a substrate material for tissue regeneration.[21]

The use of SF as substrate material in inverse opal scaffolds would not only enable fundamental cell studies on porous structures with well-defined pore sizes, but also offer an attractive biocompatible system for potential bone regeneration in vivo. SF inverse opals have been recently fabricated for photonic applications by close-packing submicrometric PMMA spheres and infiltrating them with an aqueous SF solution.[22] Although pore shape and interconnectivity could be controlled in SF scaffolds templated by paraffin globules, monodisperse pores within the size range of interest for tissue engineering applications have not yet been produced.[3] An ordered pore architecture with precisely defined pore sizes will allow for systematic fundamental studies on the influence of pore diameter and curvature on the biological response of bone-forming cells. In addition, such scaffolds might have a beneficial effect on cell viability due to enhanced diffusion or osteoblastic differentiation.[18]

This study aims at developing SF inverse opal scaffolds with monodisperse macropores in the size range of several hundred micrometers and assessing their suitability for bone tissue engineering. To evaluate its possible relevance to bone tissue engineering, we compare cell number, osteogenic differentiation capacity and extracellular matrix deposition of bone marrow derived human mesenchymal stem cells on SF inverse opals with that of conventional salt-leached scaffolds. Comparison between the spherical shape of pores for IO scaffolds and the cubic geometry of SL scaffolds also allows us to gain insights into the effect of pore geometry on osteogenesis. Based on recent studies on the 2D effect of curvature on tissue growth, we hypothesize that the pore wall curvature should also affect the cell response in the 3D environment of scaffolds and that our inverse opal scaffolds could in future be used to study the influence of geometrical parameters on engineered bone tissue.

EXPERIMENTAL
Materials
Silk cocoons from Bombyx mori L. were kindly provided by Trudel Silk Inc. (Switzerland). Lithium bromide (LiBr) and β-glycerophosphoric acid disodium salt (βGP) were obtained from Thermo Fisher Scientific (Switzerland). 1,1,1,3,3,3,-hexafluoroisopropanol (HFIP) and 2-amino-2-methyl-1-propanol (AMP) were purchased from abcr chemicals (Germany). Phosphate buffered saline (PBS) was supplied by Medicago (Sweden). Methanol and sodium hydroxide were obtained from Merck (Germany). Dulbecco's modified Eagle medium with high glucose and pyruvate (DMEM), fetal bovine serum (FBS), Trypsin-EDTA, basic fibroblastic growth factor (bFGF), non-essential amino acids, Antibiotic-Antimycotic (AntiAnti 100x) were all purchased from Gibco by Life Technologies (Switzerland). FBS Gold was supplied by PAA Laboratories (Austria). All other substances were of analytical or pharmaceutical grade and obtained from Sigma (Switzerland).

Scaffold fabrication
Salt-leached scaffold fabrication. Salt leached scaffolds were produced as described earlier.[15] In short, cocoons

from *Bombyx Mori L.* were boiled twice for 1 h in 0.02M Na_2CO_3 solution. Boiled SF was rinsed with ultrapure water (UPW) and dried at room temperature in a fume hood. On the next day, a 10% (w/v) solution of SF in 9M LiBr was produced and dialyzed against UPW for 36 h. The resulting solution was filtered using a 5 μm syringe filter, frozen at −80°C overnight and lyophilized in a lyophilizer (Alpha 1–2, Martin Christ GmbH, Germany) for 5 days. With the lyophilized SF a 17% (w/v) solution in HFIP was produced. The dissolved SF was then added to NaCl crystals with a granule diameter between 300 and 400 μm (1 mL solution to 2.5 g NaCl crystals). After 3 days of HFIP evaporation the silk-salt blocks were treated for 30 min with 90% MeOH solution to induce crystallization into β-sheet conformation.[23] NaCl was leached from the dried scaffolds by immersing the silk-salt blocks in UPW for 2 days. Scaffolds were cut by hand with a razor blade to a thickness of 5 mm and punched with a skin biopsy punch to disks with a diameter of 5 mm. Scaffolds were sterilized while immersed in PBS by steam-autoclaving at 121°C and 1 bar for 20 min.

Inverse opal scaffold fabrication. A schematic describing the inverse opal fabrication process in detail can be found in the supplementary information (Supporting Information Fig. S1). A glass capillary microfluidic device was assembled as described previously.[24] Briefly, the emitter was produced by pulling a borosilicate round glass capillary (1 mm outer diameter, World Precision Instruments, Germany) using a pipette-puller (Flaming/Brown micropipette puller model P-97, Sutter Instruments, USA). The opening of the pulled capillary was adjusted to 300 μm by grinding on sandpaper. Unpulled round capillaries with an inner diameter of 580 μm were used as collectors. The two round capillaries were aligned inside a square capillary (inner diameter 1.05 mm, outer diameter 1.5 mm, Harvard, USA) and glued onto glass slides using a two-component epoxy. Syringe tips (I and Peter Gonano, Austria) were placed at both ends of the square capillary as inlets and were fixed with epoxy. Poly-ethylene tubes (Scientific Commodities Inc, USA) connected the inlets with glass syringes (Hamilton Gastight, Switzerland) placed in syringe pumps (PHD2000, Harvard Apparatus, USA).

A 10% (w/w) poly(caprolactone) (PCL) solution in dichloromethane and a 2% (w/w) poly(vinyl alcohol) (PVA) solution in water were used as inner and outer phase, respectively. Flow rates were adjusted to 5 mL/h for the inner and 8 mL/h for the outer phase. The droplets were collected in an excess of PVA solution and left resting for ∼5 weeks to slowly evaporate the dichloromethane. After washing 5 times in water and once in ethanol, the particles were placed in molds (4 mm diameter, 4 mm in height), slightly agitated to close pack and dried. To induce necking between the particles, they were heated to 57°C at 25% RH in a climate chamber (HCP108, Memmert, Germany) for 1 h. A 12% (w/w) SF solution was prepared by dissolving lyophilized SF in UPW, following the protocol described in the previous section for the fabrication of salt-leached scaffolds. 100 μL of the aqueous SF solution were infiltrated into each

particle pack and let dry. Following 1 h exposure to 90% methanol to crystallize the SF, the porogen particles were removed in dichloromethane for 8 h and finally washed in ethanol to remove any solvent residues and left to dry.

For cell experiments, scaffolds were immersed in PBS and steam-sterilized at 121°C and 1 bar for 20 min.

Scaffold characterization

Porosity and pore diameter distribution. Inverse opal and salt leached scaffolds ($n = 5$ per group) were scanned dry in a micro-computed tomograph (μCT 40, SCANCO Medical AG, Brüttisellen, Switzerland) at a voxel resolution of 6 μm. The energy level was set to 45 kVp, the intensity to 177 μA, the integration time to 200 ms and a 4-fold frame-averaging was applied. A cylindrical volume of interest (VOI) of 2.16 mm in diameter and 2.55 mm in height corresponding to half the mean scaffold diameter and half the mean scaffold height was defined for further evaluation. To reduce noise, the VOI was Gaussian filtered using a filter width of 1.2 and a support of 1. Gray-scale VOIs were binarized using a threshold of 5.5% maximal gray-scale value. Unconnected particles were removed for further evaluation. The resulting 3D volume was evaluated for porosity, pore diameter distribution and surface density as described in Ref. 25. Briefly, the porosity was calculated by dividing the volume occupied by the pores within the solid scaffold by the volume evaluated in percentage. Pore sizes were determined using the distance transformation method and pore diameter distribution was determined by plotting pore sizes against the number of voxels within pores of the corresponding size. Finally, the surface density was computed by dividing the surface of the volume occupied by the scaffold by the volume evaluated.[26]

Mechanical properties. Before testing, scaffolds were boiled in PBS for 20 min to ensure that they were fully hydrated and then left to equilibrate to ambient temperature. Scaffolds were cylindrical with a diameter and a thickness of 5 mm. Unconfined compression tests ($n = 5$ per group) in the wet state were then performed on a mechanical tester (Instron 4411, Germany) equipped with a 10 N load cell at a crosshead speed of 0.5 mm/min. To extract the elastic modulus, a linear fit of the stress−strain curve between 0.15 and 2 kPa was performed.

To eliminate the effect of porosity and estimate the elastic modulus of the pore struts alone, we utilized the following equation derived by Gibson and Ashby[27]: $E^*/E^s = (\rho^*/\rho^s)^2$, where E^* is the measured scaffold modulus, E^s is the modulus of the single SF strut, ρ^* is the scaffold's density and ρ^s is the SF pore-free density. Assuming the ratio ρ^*/ρ^s to be equal to 1 - P, the elastic modulus E^s was calculated for both scaffold types.

Silk fibroin morphology. Infrared spectra were obtained on an ATR FTIR (Cary 670 FTIR Spectrometer, Agilent Technologies, USA). 256 scans at a resolution of 2 cm^{-1} were performed for each sample.

Cell culture

HMSCs were isolated and characterized from bone marrow of healthy donors (Lonza, United States) as described previously.[1] Passage 3 cells were expanded for 7 days in expansion medium based on DMEM containing 10% FBS and 1% antibiotic-antimycotic, 1% nonessential amino acids and 1 ng/mL basic fibroblast growth factor. After trypsinization, cells were counted and seeded at a density of 10^6 cells/scaffold and cultured in control medium consisting of DMEM with 10% FBS (PAA Gold) and 1% AntiAnti. The medium was exchanged three times a week. To induce osteogenic differentiation, an osteogenic medium, where the control medium was supplemented with 50 μg/mL ascorbic acid, 100 nM dexamethasone and 10 mM β-glycerophosphate, was applied instead of the pure control medium. All constructs were kept at 37°C, 5% CO_2 and 100% relative humidity throughout the study.

Biochemical characterization

Cell metabolic activity. After 2, 4 and 6 weeks in culture, cell metabolic activity was measured by the AlamarBlue® assay (Lucerna-Chem AG, Switzerland) using 1.5 mL of a 10% (v/v) solution of AlamarBlue® reagent in control or osteogenic medium for scaffolds cultured in control or osteogenic medium, respectively. After an incubation time of 3 h in 24-well plates, fluorescence at an excitation wavelength of 560 nm and an emission wavelength of 590 nm was measured ($n = 4$ per group). The measured activity was then normalized by the DNA content measured on the identical scaffold.

Cell number. After culture, scaffolds of all groups were washed in PBS and disintegrated in 0.5 mL of 0.2% (v/v) Triton X-100 and 5 mM $MgCl_2$ solution using steel beads and a Mini Beadbeater™ (Biospec, USA). After 48 h incubation at room temperature, the solids were separated by centrifugation at 3000g for 10 min. With the supernatant, the Quant-iT™ PicoGreen assay (Life Technologies, Switzerland) was carried out according to the manufacturer's instructions ($n = 4$ per group). Cell number was evaluated after 2, 4, or 6 weeks in culture.

Alkaline phosphatase activity. Alkaline phosphatase measurements were carried out directly after culture (2, 4, or 6 weeks) with scaffolds that had been disintegrated as described in the previous section. Identical scaffolds were used for both assays. In a 96-well plate 80 μL of the supernatant were mixed with 20 μL of 0.75M AMP buffer and 100 μL 100 mM p-nitrophenylphosphate solution and incubated for 2 min, before adding 0.2M NaOH to stop the conversion of p-nitrophenylphosphate to p-nitrophenol. Absorbance at 405 nm was measured and ALP activity was calculated by comparison to standards of known p-nitrophenol concentration. The calculated alkaline phosphatase activity was then normalized by the DNA content measured for each scaffold.

Calcium content. Four scaffolds per group were washed in PBS, decomposed in 0.5 mL of 5% (w/v) trichloroacetic acid in UPW each using stainless steel balls and a Mini Beadbeater™ and incubated for 48 h at room temperature to extract the calcium. After removal of the solids by centrifugation at 3000g for 10 min, a colorimetric calcium assay (Calcium CPC FS, Rolf Greiner BioChemica, Germany) was performed according to the manufacturer's instructions. Measurements were conducted after 2, 4, or 6 weeks in culture.

SEM. After 6 weeks in culture, constructs ($n = 2$ per group) were fixed in 2.5% (v/v) glutaraldehyde in 0.1M cacodylate buffer for 4 h. After rinsing with 0.1M cacodylate buffer they were placed in 0.04% osmium tetroxide in 0.1M cacodylate buffer for 90 min. Scaffolds were rinsed with cacodylate buffer again prior to dehydration in a graded ethanol series and were subsequently frozen at -80°C and lyophilized. All samples were sputter-coated (SCD500, Baltec, Liechtenstein) with a thin platinum layer before observation in the SEM (LEO Gemini 1530, Zeiss, Germany).

Histology. After 6 weeks in culture, scaffolds ($n = 2$ per group) were fixed in 10% neutral buffered formalin overnight and subsequently dehydrated in an automatic tissue processor (TCP 15 Duo, Medite AG, Switzerland) and embedded in paraffin. Sections of 5 μm in thickness were cut with a microtome (HM355S, Microm International GmbH, Germany). The sections were then stained with haematoxylin and eosine (H&E), mounted with Cytoseal (Cytoseal™ 280, Richard-Allan Scientific, USA) and observed under a light microscope (DMIL LED, Leica, Switzerland).

Statistical analysis. Statistical analysis was performed in SPSS Statistics 22 (IBM, Switzerland). Analysis of variance was applied to identify statistically significant factors. Post-hoc Bonferroni tests were carried out for direct comparison between groups. $p < 0.05$ was considered as statistically significant. All results are displayed as mean values $\pm$ standard deviation.

RESULTS

The porous architectures of salt-leached (SL) and inverse opal scaffolds were considerably different with regards to pore shape and regularity [Figure 1(a,b)]. Due to the morphological nature of the NaCl particles used as pore templates, the salt-leached scaffold exhibited a microstructure with faceted pores. The salt crystals used as pore templates in this study were intentionally sieved in order to obtain SL scaffolds with a relatively narrow pore size distribution in the range from 300 to 400 μm. A more regular and homogeneous structure was observed in the inverse opal scaffolds, where the pores were generated by spherical PCL particles. Figure 1(c,d) shows the pore walls of SL and IO scaffolds, respectively. Both scaffold types show some roughness on a similar micrometer scale. The diameter distribution of the scaffolds as determined by microCT revealed a larger size for salt-leached scaffolds as opposed to the inverse opals (mean pore diameter: 231 ± 18 vs. 171 ± 7 μm, $p < 0.001$).
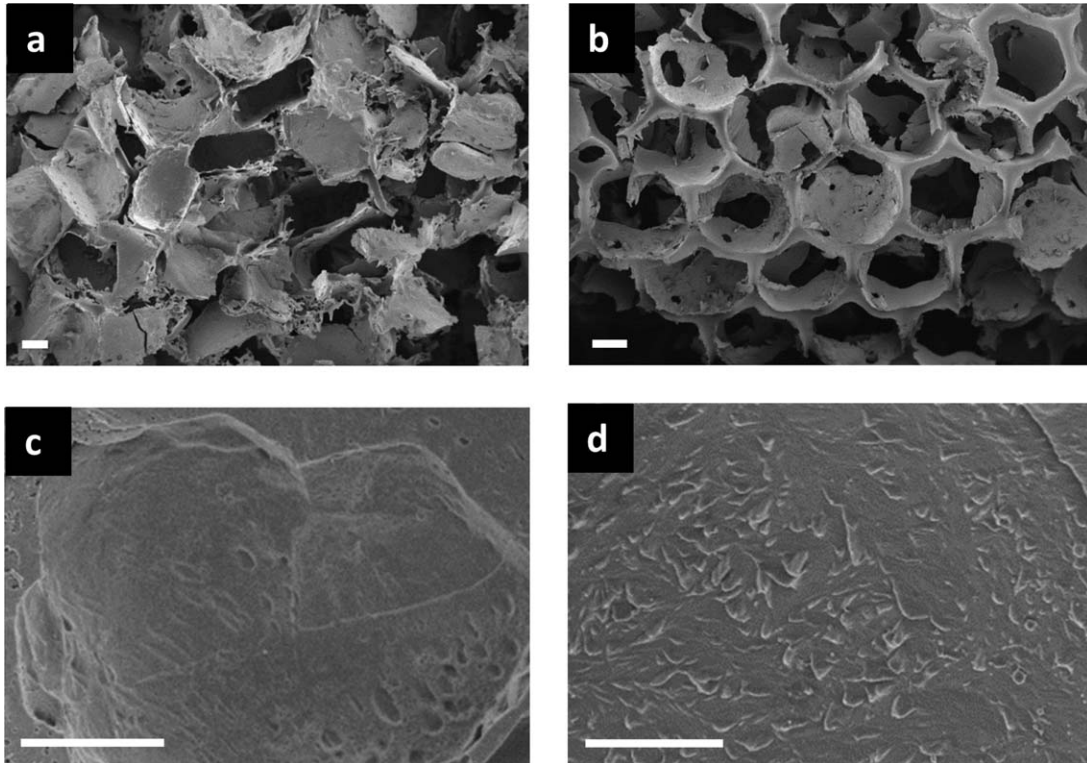
FIGURE 1. SEM micrographs showing the pore architecture of salt-leached (a) and inverse opal (b) SF scaffolds. Scale bar in (a,b) 100 μm. Pore wall morphology is displayed in (c) for salt-leached and (d) for inverse opal scaffolds. Scale bar in (c,d) 10 μm.

More remarkably, however, the scaffolds differ in diameter distribution, with pore diameters detected by microCT ranging from 6 to 678 μm and 6 to 312 μm for SL [Figure 2(a)] and IO [Figure 2(b)] scaffolds, respectively. That is, pore diameters cover more than double the size range for salt-leached scaffolds as compared to inverse opals. Representative 3D reconstructions obtained for the scanned scaffolds are displayed in Figure 2(a,b).

The different pore morphologies in SL and IO structures resulted in scaffolds with distinct architectures. Because of the tighter packing of faceted porogens, SL structures display higher porosity after removal of the salt template. Porosities calculated from the microCT scans led to values of $92.8 \pm 0.6\%$ for the SL and $84.7 \pm 2.1\%$ ($p < 0.001$) for the IO scaffolds [Figure 2(c)]. As a result the normalized scaffold surface area (BS/TV) in the SL was significantly smaller than in the IO (9.5 ± 0.5 vs. 13.2 ± 0.6, $p < 0.01$).

The porosity level is known to significantly affect the elastic modulus of the scaffold. Indeed, the compressive elastic modulus (E^*) of the more porous SL structure in the wet state was found to be 4.16 ± 0.87 kPa, as opposed to the value of 12.63 ± 5.54 kPa measured for the IO scaffolds ($p < 0.05$) [Figure 3(a)]. Interestingly, an E^s value of 834.30 kPa representing the pore wall modulus was obtained for the SL scaffolds. This is about 50% higher than the estimated elastic modulus of the walls in the IO structure (539.32 kPa), but the difference was not significant ($p > 0.05$). Although the experimental elastic moduli used in these calculations are also expected to be affected by the different pore morphologies of the scaffolds, we conclude from these estimates that the struts exhibited stiffnesses within the same order of magnitude for the two investigated structures.

Despite the differences in the two fabrication processes, the SF in both scaffolds displayed very similar molecular conformation as confirmed by infrared spectroscopy [Figure 3(b)]. The peak at 1620 cm^{-1} confirmed the presence of crystalline β-sheets in both SL and IO scaffolds.[28] In both fabrication processes scaffolds were methanol-treated leading, as expected, to silk fibroin crystallization, since methanol is well known to induce the formation of β-sheets in silk fibroin.[28]

The effect of the SL and IO porous architectures on the biological response of hMSC was investigated by analyzing cell number via DNA content, cell metabolic activity, osteogenic differentiation via alkaline phosphatase activity and mineralization by colorimetric calcium assay over a culture period of 6 weeks. Tissue distribution and morphology were studied through SEM observation and optical microscopy of histological sections.

No significant difference in DNA content per scaffold was measured between the salt-leached and the inverse opal scaffolds cultured in osteogenic medium within the first 6 weeks (Figure 4). This indicates that initial cell attachment and proliferation was comparable for the two architectures. However, in control medium statistically significantly lower DNA contents were observed as compared to osteogenic medium for salt-leached scaffolds after 2
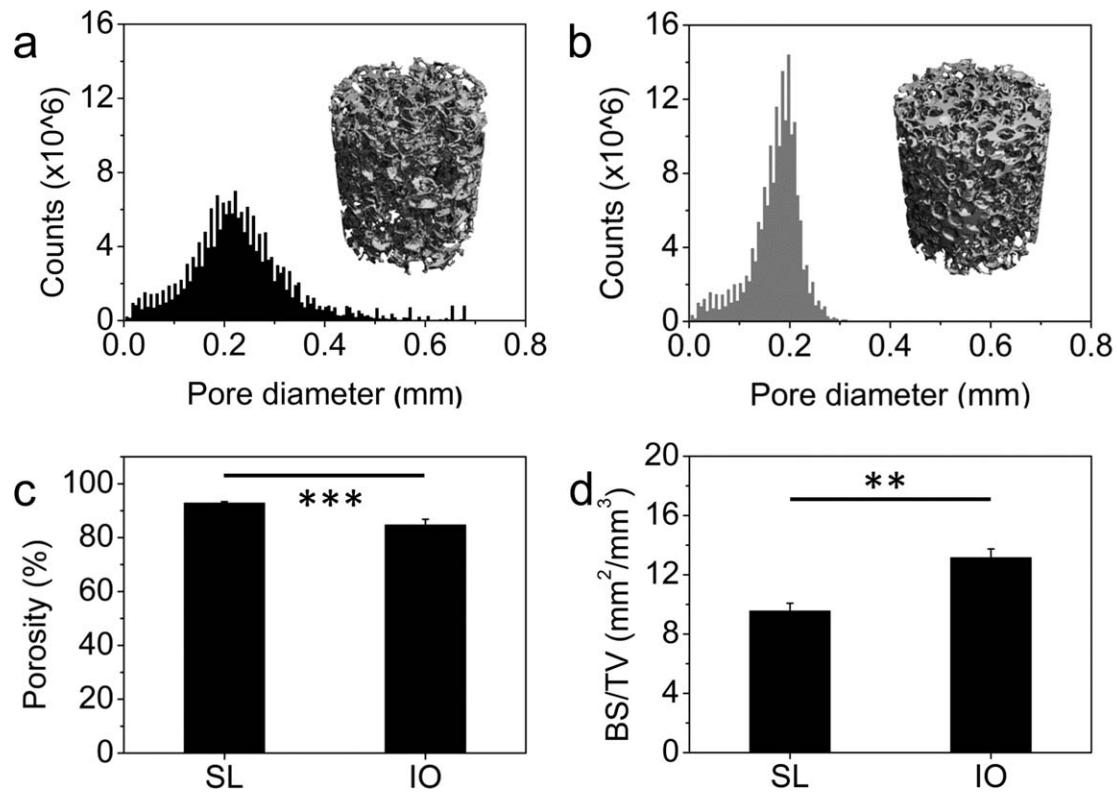
FIGURE 2. Pore diameter distribution and a representative 3D reconstruction of salt-leached scaffolds (a) and inverse opal scaffolds (b) as determined by microCT measurements. Porosity (c) and scaffold surface area normalized by the total scaffold volume (d) calculated from the scans for salt-leached and inverse opal scaffolds. $*p < 0.05$, $**p < 0.01$, $***p < 0.001$.
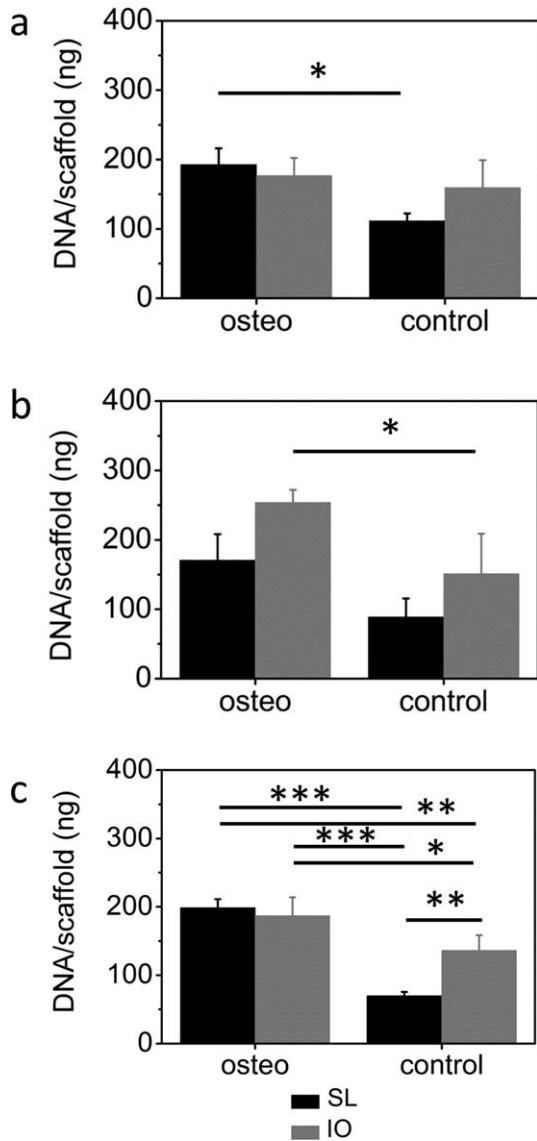
weeks (112 ± 11 vs. 193 ± 24 ng, $p < 0.05$) as well as for the inverse opals after 4 weeks (151 ± 58 vs. 254 ± 18 ng, $p < 0.05$) [Figure 4(a,b)]. After 6 weeks, significant differences between scaffolds in osteogenic and control medium (salt-leached: 199 ± 13 vs. 70 ± 6 ng, $p < 0.001$, inverse opal: 187 ± 27 vs. 137 ± 22 ng, $p < 0.05$), as well as between scaffold types in control medium (70 ± 6 vs. 137 ± 22 ng, $p < 0.01$), were observed [Figure 4(c)]. Prolonged static culture led to a decrease in cell number on control scaffolds, which was more pronounced on the salt-leached scaffolds leading to a significant difference in week

6. Contrarily, no decline was observed in osteogenic scaffolds, which displayed similar cell numbers after 6 weeks in culture.
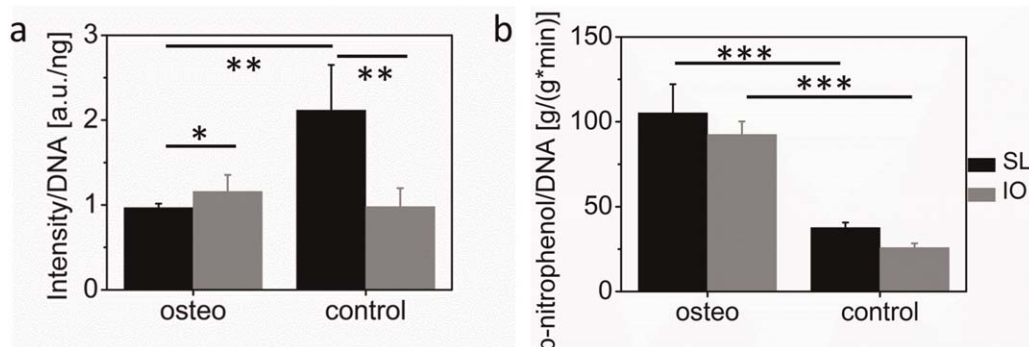
The viability of cells within the scaffolds was confirmed by following their metabolic activity using the AlamarBlue™ assay normalized to the amount of cells in the respective sample [Figure 5(a) and Supporting Information S2]. The cell metabolic activity in the first 4 weeks was significantly higher on salt-leached scaffolds than on inverse opals in control medium (Supporting Information Figure S2b). At the earliest measurement point after 2 weeks in culture, there
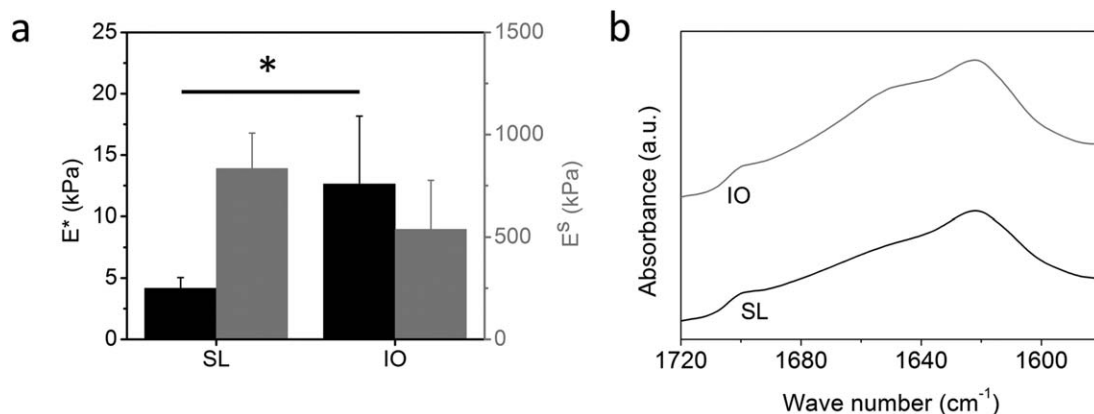
FIGURE 3. (a) Elastic moduli in compression (black columns) and calculated pore wall stiffness (gray columns) of the wet silk fibroin scaffolds. $*p < 0.05$. (b) ATR-FTIR spectra obtained for the salt-leached and inverse opal scaffolds in the amide I region showing their crystallinity.

FIGURE 4. Amount of DNA per scaffold measured after (a) 2, (b) 4, and (c) 6 weeks in culture for salt-leached (black columns) and inverse opal (gray columns) scaffolds are shown. $*p < 0.05$, $**p < 0.01$, $***p < 0.001$.

was also a significant difference between osteogenic and control medium for salt-leached scaffolds (Supporting Information Figure S2a), which was not present in week 4. At week 6, the hMSCs cultured on the salt-leached scaffold in control medium showed higher cell metabolic activity than on the inverse opals (2.12 ± 0.53 vs. 0.98 ± 0.22, $p < 0.01$) and also higher than on the scaffolds in osteogenic medium (0.97 ± 0.08, $p < 0.01$ and 1.16 ± 0.20, $p < 0.05$ for salt leached and inverse opal, respectively) [Figure 5(a)].

To obtain information on the osteogenic differentiation of the stem cells, alkaline phosphatase (ALP) activity was measured as depicted in Figure 5(b). The obtained values were normalized by the DNA content measured on the very same scaffolds [Figure 4(a)]. Only ALP activities measured after 2 weeks in culture are shown here, because ALP is an early marker for osteogenic differentiation. Values measured at later time points are shown in Supporting Information Figure S3. Since ALP is an ubiquitous enzyme present on most cell membranes, positive ALP values were measured for both osteogenic and control cultures. However, ALP activity in week 2 was significantly higher for cells in osteogenic medium than in control medium [Figure 5(b)]. Salt-leached and inverse opal scaffolds in osteogenic media exhibited values of 105.28 ± 16.89 and 92.54 ± 7.72 g/(g*min), respectively. These activity data were significantly higher ($p < 0.001$) than the values of 37.60 ± 3.09 and 25.83 ± 2.45 g/(g*min) measured for the salt-leached and inverse opals in control medium, respectively. Such results indicate that hMSCs only underwent differentiation in osteogenic culture medium.

After differentiation into the osteogenic lineage, cells are expected to promote mineralization through the induced precipitation of calcium phosphate from the culture medium. To assess possible mineralization of the scaffolds, we measured the calcium content of samples cultured for 2, 4, or 6 weeks. After 2 weeks in culture, calcium was undetectable in both scaffold types, regardless if cells were cultured in osteogenic or control medium. At week 4 [Figure 6(a)], a significantly higher calcium content was observed in inverse opal scaffolds under osteogenic medium as compared to the control (1417.13 ± 734.17 vs. 0 ± 0 μg,

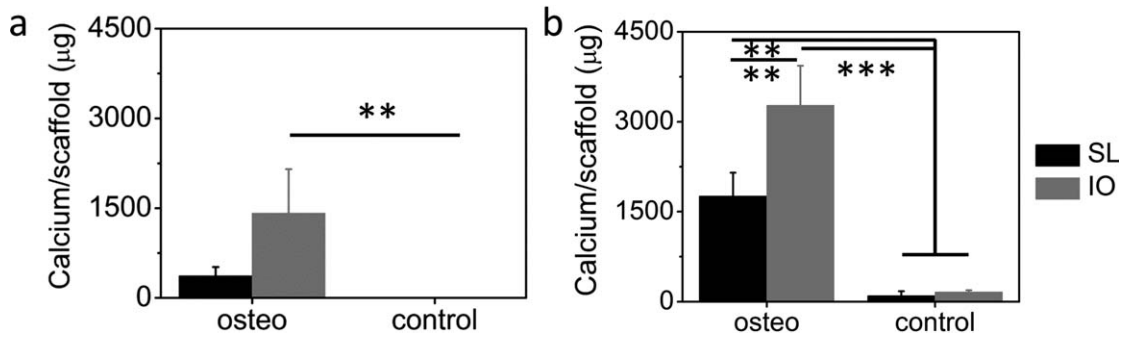FIGURE 5. Cell metabolic activity as measured by AlamarBlueTM at week 6 (a) and alkaline phosphatase activity determined by the conversion of p-nitrophenolphosphate to p-nitrophenol (b) for salt-leached (black columns) and inverse opal (gray columns) scaffolds after 2 weeks in culture in osteogenic or control medium. $*p < 0.05$, $**p < 0.01$, $***p < 0.001$.

FIGURE 6. Calcium content measured after 4 (a) and 6 (b) weeks in culture for salt-leached (black columns) and inverse opal (gray columns) scaffolds cultured in osteogenic or control medium. $*p < 0.05$, $**p < 0.01$, $***p < 0.001$.

$p < 0.01$). This was not the case for the salt-leached constructs (386.48 ± 147.50 vs. 0 ± 0 μg, $p > 0.05$). Two weeks later, however, both scaffold types showed significantly more mineralization in osteogenic medium in comparison to control medium [Figure 6(b)]. Most importantly, the total calcium content after 6 weeks was significantly higher on the inverse opal scaffolds than on the salt-leached ones: 3275.49 μg ± 662.29 for IO samples as opposed to 1760.72 ± 389.52 μg for SL specimens ($p < 0.01$).

The presence of calcium after 6 weeks of culture in osteogenic medium indicates that cells have produced mineralized extracellular matrix within the scaffolds during this time period. The morphology of the new tissue comprising cells and mineralized matrix within the two types of scaffolds was examined by SEM (Figure 7). Denser tissue almost

filled individual pores in the osteogenic scaffolds, whereas the stem cells and their matrix appear more fibrous and less dense in control medium. This suggests that there was a higher degree of tissue growth in osteogenic medium, which correlated well with the higher cell number measured under this condition (Figure 4). The higher magnification images shown in the insets of Figure 6 provided further evidence of the distinct tissue morphology obtained for scaffolds in osteogenic and control media. No cells or extracellular matrix could be found on scaffolds without seeded cells (data not shown here).

H&E stained sections were imaged after 6 weeks in culture (Figure 8). They confirmed that in both osteogenic and control medium tissue grew well into the pores of both scaffold types, showing a rather even cell distribution.
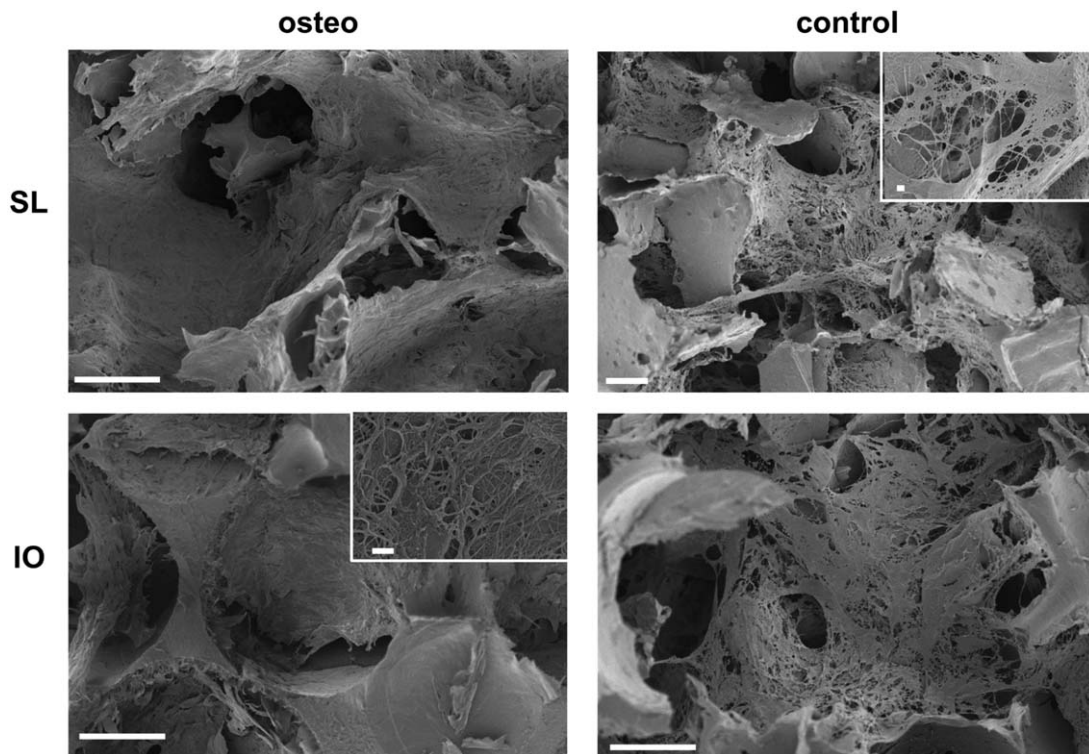
FIGURE 7. SEM images of salt-leached and inverse opal SF scaffolds after 6 weeks in culture in osteogenic and control medium. Representative insets show tissue morphology. Scale bars 100 μm, scale bars in insets 1 μm.
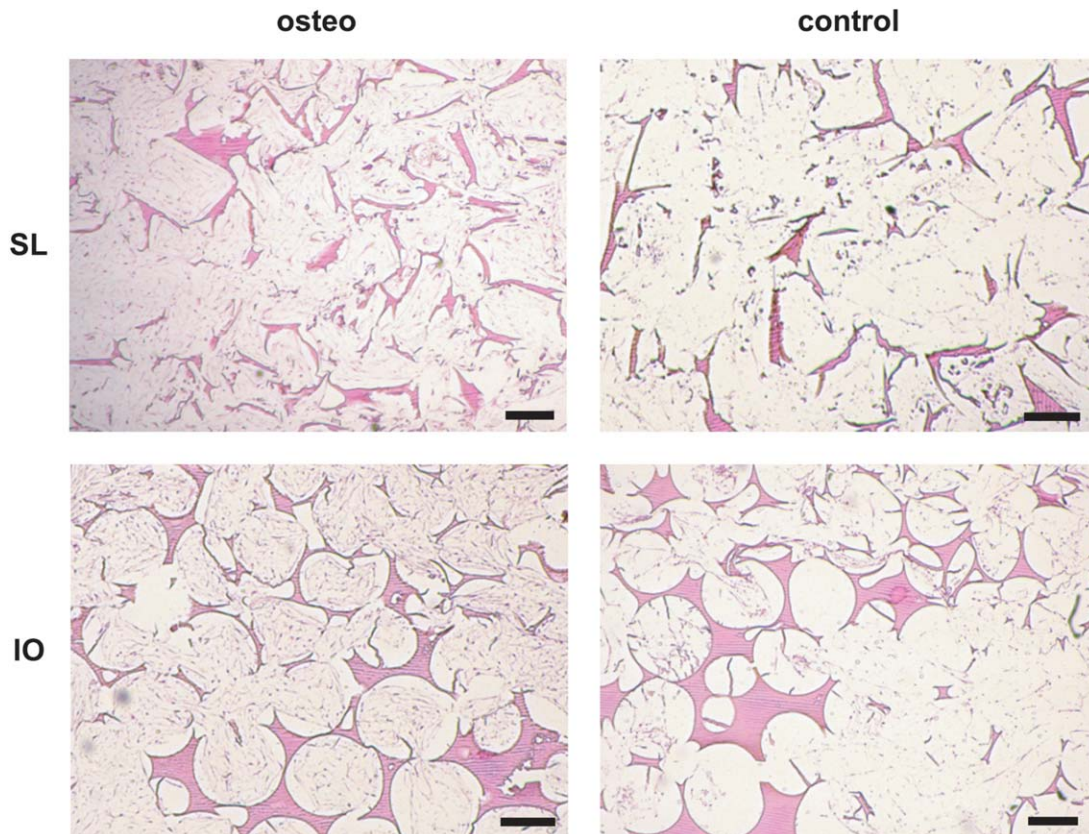
FIGURE 8. H&E stained sections of salt-leached and inverse opal scaffolds cultured for 6 weeks in osteogenic or control medium. Scale bars are 200 μm.

Qualitatively, the amount of cells appeared to be smaller in the control scaffolds than in the osteogenic, which is confirmed by DNA content measurements (Figure 4).

DISCUSSION

In this study, inverse opal scaffolds with controlled and homogeneous architectures have been developed and compared to widespread salt-leached SF scaffolds. Because of distinct fabrication processes, the two types of scaffolds varied in a number of structural properties. After a culture period of 6 weeks, similar cell number and cell metabolic activity as well as ALP activity were observed in osteogenic medium for both scaffolds. But, most notably, the amount of mineralization was significantly higher (almost doubled) for inverse opal scaffolds.

To discuss possible factors leading to the considerable variation in calcium content measured between the two scaffold types, we analyzed the potential influence of several scaffold-dependent parameters on hMSC differentiation, extracellular matrix deposition, and mineralization. The investigated physical parameters that might exert an effect on the calcium phosphate deposition were the morphology including average pore diameter, pore diameter distribution, porosity, scaffold surface area, scaffold elastic modulus, pore wall stiffness, and the microtopography of the pore walls.

A monodisperse pore diameter distribution was shown to promote osteogenic differentiation as determined by ALP activity.[18] However, no studies were performed yet that compared mineralization in scaffolds with varying pore diameter distribution while keeping a similar mean pore diameter. Hence, drawing conclusions on how pore diameter distribution influences mineralization in scaffolds and whether there is a pore diameter that allows for optimal cell infiltration and extracellular matrix mineralization remains speculative.

The observed difference in scaffold porosity and normalized surface area available to the cells could have led to a higher initial cell number in the inverse opal scaffolds. Higher cell seeding density was shown in the literature to influence mineralization at an early stage but not at later time points.[29]

The pore diameter range used here, namely around 200 μm, is relatively large compared to the cell's size. Therefore, the wall curvature experienced by hMSCs is minimal and is not expected to affect cell behavior regardless of the exact scaffold geometry.[30] On the tissue level, local pore curvature is known to affect the tissue growth mechanism but not the total amount of tissue deposited after a certain time in culture for similar concave pore diameters.[6] It has been shown, however, that a wavy surface structure could induce bone formation on hydroxyapatite-coated titanium implants but not on flat controls.[31] Thus, the different pore shapes in the two examined scaffolds might have contributed to the increased mineralization.

The elastic modulus of the scaffold is an important physical property that determines the potential use of the synthetic construct in load-bearing applications. Ideally, at least in an approach mimicking the physiological tissue, it should lie in the range of 10 to 20 GPa, which is the elastic modulus of bone.[32] However, cells likely probe and respond to the local pore wall stiffness rather than the scaffold modulus. Although the scaffold elastic modulus measured in compression was higher for inverse opal scaffolds, the pore walls of salt-leached scaffolds were found to be 50% stiffer when the properties of the porous construct were corrected for porosity. The difference in pore wall modulus may be explained by variations in solvents, solution concentrations or the influence of porogen particles used in the distinct scaffold fabrication processes. While elastic moduli similar to those of various native tissues within 0.1 and 59 kPa were shown to impact stem cell response both in 2D and 3D,[7,33] the values of 834 kPa and 539 kPa measured in our study for the silk pore wall moduli E^s lay well above that range. Hence, scaffold stiffness was most probably not the main cause for the observed increased mineralization, especially considering the higher modulus obtained for salt-leached scaffolds.

A change in conformation in SF has been shown to influence cell behavior through a difference in nanotopography.[34] However, peaks that can be attributed to β-sheets were visible in the IR spectra of both scaffold types and are thus not suggested to affect cell response here. Additionally, scaffold surface roughness is also dependent on the smoothness and surface area of the porogen. Relatively smooth pore walls were found for both scaffold types as indicated by SEM imaging (Figure 1). Thus, the effect of surface roughness on mineralization is likely negligible here.

One of the difficulties in studying the influence of scaffold parameters on cell response is that it is often very challenging to tune a single factor in a 3D scaffold without also affecting other features. For instance, changing to a narrower pore diameter distribution and different pore shape in this study inevitably led to a decrease in porosity. Hence, identifying the ideal parameters a scaffold should exhibit is not trivial. Here, we discussed several factors that might have potentially caused the higher mineralization in the inverse opal scaffolds. Drawing a definite conclusion requires further studies focused on each one of the structural features identified in this work. It is probable that an interplay of more than one of the discussed factors affected the tissue growth over the time course of the study.

CONCLUSION

Increased mineralization of hMSC was observed on newly developed silk fibroin inverse opal scaffolds when compared to salt-leached scaffolds despite a similar cell number measured on both structures. Several architectural and material factors of the two scaffold types have been examined and carefully analyzed in terms of their potential influence on stem cell behavior and eventually extracellular matrix deposition and mineralization. While stiffness and topography of the two scaffolds were comparable, they greatly differed in a number of architectural properties, notably pore shape, diameter distribution and overall porosity. In the inverse opals, these structural parameters were found to lie within a range that positively influences the mineralization of the scaffold. Our systematic evaluation of architectural and physical factors that may affect scaffold mineralization should be continued in future work to enable a closer investigation of these effects in order to design scaffolds that promote bone regeneration.

REFERENCES
1. Hofmann S, Hagenmuller H, Koch AM, Muller R, Vunjak-Novakovic G, Kaplan DL, et al. Control of in vitro tissue-engineered bone-like structures using human mesenchymal stem cells and porous silk scaffolds. Biomaterials 2007;28:1152–1162.
2. Hofmann S, Knecht S, Langer R, Kaplan DL, Vunjak-Novakovic G, Merkle HP, et al. Cartilage-like tissue engineering using silk scaffolds and mesenchymal stem cells. Tissue Eng 2006;12:2729–2738.
3. Uebersax L, Hagenmueller H, Hofmann S, Gruenblatt E, Mueller R, Vunjak-Novakovic G, et al. Effect of scaffold design on bone morphology in vitro. Tissue Eng 2006;12:3417–3429.
4. Thimm BW, Wust S, Hofmann S, Hagenmuller H, Muller R. Initial cell pre-cultivation can maximize ECM mineralization by human mesenchymal stem cells on silk fibroin scaffolds. Acta Biomater 2011;7:2218–2228.
5. Karageorgiou V, Kaplan D. Porosity of 3D biornaterial scaffolds and osteogenesis. Biomaterials 2005;26:5474–5491.
6. Rumpler M, Woesz A, Dunlop JWC, van Dongen JT, Fratzl P. The effect of geometry on three-dimensional tissue growth. J R Soc Interface 2008;5:1173–1180.
7. Engler AJ, Sen S, Sweeney HL, Discher DE. Matrix elasticity directs stem cell lineage specification. Cell 2006;126:677–689.
8. Kumar G, Waters MS, Farooque TM, Young MF, Simon CG. Free-form fabricated scaffolds with roughened struts that enhance both stem cell proliferation and differentiation by controlling cell shape. Biomaterials 2012;33:4022–4030.
9. Meinel L, Karageorgiou V, Fajardo R, Snyder B, Shinde-Patil V, Zichner L, et al. Bone tissue engineering using human mesenchymal stem cells: Effects of scaffold material and medium flow. Annals Biomed Eng 2004;32:112–122.
10. Karageorgiou V, Meinel L, Hofmann S, Malhotra A, Volloch V, Kaplan D. Bone morphogenetic protein-2 decorated silk fibroin films induce osteogenic differentiation of human bone marrow stromal cells. J Biomed Mater Res Part A 2004;71:528–537.
11. Meinel L, Fajardo R, Hofmann S, Langer R, Chen J, Snyder B, et al. Silk implants for the healing of critical size bone defects. Bone 2005;37:688–698.
12. Meinel L, Karageorgiou V, Hofmann S, Fajardo R, Snyder B, Li CM, et al. Engineering bone-like tissue in vitro using human bone marrow stem cells and silk scaffolds. J Biomed Mater Res Part A 2004;71:25–34.
13. Altman GH, Diaz F, Jakuba C, Calabro T, Horan RL, Chen JS, et al. Silk-based biomaterials. Biomaterials 2003;24:401–416.
14. Hofmann S, Hilbe M, Fajardo RJ, Hagenmuller H, Nuss K, Arras M, et al. Remodeling of tissue-engineered bone structures in vivo. Eur J Pharm Biopharm 2013;85:119–129.
15. Nazarov R, Jin HJ, Kaplan DL. Porous 3-D scaffolds from regenerated silk fibroin. Biomacromolecules 2004;5:718–726.
16. Joao CFC, Vasconcelos JM, Silva JC, Borges JP. An overview of inverted colloidal crystal systems for tissue engineering. Tissue Eng Part B-Rev 2014;20:437–454.
17. Choi SW, Zhang Y, Thomopoulos S, Xia YN. In vitro mineralization by preosteoblasts in poly(DL-lactide-co-glycolide) inverse

opal scaffolds reinforced with hydroxyapatite nanoparticles. Langmuir 2010;26:12126–12131.

18. Choi SW, Zhang Y, Xia YN. Three-dimensional scaffolds for tissue engineering: The importance of uniformity in pore size and structure. Langmuir 2010;26:19001–19006.

19. Galperin A, Oldinski RA, Florczyk SJ, Bryers JD, Zhang MQ, Ratner BD. Integrated bi-layered scaffold for osteochondral tissue engineering. Adv Healthc Mater 2013;2:872–883.

20. Cuddihy MJ, Kotov NA. Poly(lactic-co-glycolic acid) bone scaffolds with inverted colloidal crystal geometry. Tissue Eng Part A 2008;14:1639–1649.

21. Fu K, Pack DW, Klibanov AM, Langer R. Visual evidence of acidic environment within degrading poly(lactic-co-glycolic acid) (PLGA) microspheres. Pharm Res 2000;17:100–106.

22. Kim S, Mitropoulos AN, Spitzberg JD, Tao H, Kaplan DL, Omenetto FG. Silk inverse opals. Nat Photonics 2012;6:817–822.

23. Tsukada M, Gotoh Y, Nagura M, Minoura N, Kasai N, Freddi G. Structural-changes of silk fibroin membranes induced by immersion in methanol aqueous-solutions. J Polym Sci B-Polym Phys 1994;32:961–968.

24. Studart AR, Studer J, Xu L, Yoon K, Shum HC, Weitz DA. Hierarchical porous materials made by drying complex suspensions. Langmuir 2011;27:955–964.

25. van Lenthe GH, Hagenmuller H, Bohner M, Hollister SJ, Meinel L, Muller R. Nondestructive micro-computed tomography for biological imaging and quantification of scaffold-bone interaction in vivo. Biomaterials 2007;28:2479–2490.

26. Hildebrand T, Laib A, Muller R, Dequeker J, Ruegsegger P. Direct three-dimensional morphometric analysis of human cancellous bone: Microstructural data from spine, femur, iliac crest, and calcaneus. J Bone Miner Res 1999;14:1167–1174.

27. Gibson MFA. Cellular Solids—Structure and Properties, 2nd ed. Cambridge: Cambridge University Press; 1997.

28. Hu X, Kaplan D, Cebe P. Determining beta-sheet crystallinity in fibrous proteins by thermal analysis and infrared spectroscopy. Macromolecules 2006;39:6161–6170.

29. Holy CE, Shoichet MS, Davies JE. Engineering three-dimensional bone tissue in vitro using biodegradable scaffolds: Investigating initial cell-seeding density and culture period. J Biomed Mater Res 2000;51:376–382.

30. Peyton SR, Kalcioglu ZI, Cohen JC, Runkle AP, Van Vliet KJ, Lauffenburger DA, et al. Marrow-derived stem cell motility in 3D synthetic scaffold is governed by geometry along with adhesivity and stiffness. Biotechnol Bioeng 2011;108:1181–1193.

31. Ripamonti U, Roden LC, Renton LF. Osteoinductive hydroxyapatite-coated titanium implants. Biomaterials 2012;33: 3813–3823.

32. Rho JY, Ashman RB, Turner CH. Youngs modulus of trabecular and cortical bone material - Ultrasonic and microtensile measurements. J Biomech 1993;26:111–119.

33. Parekh SH, Chatterjee K, Lin-Gibson S, Moore NM, Cicerone MT, Young MF, et al. Modulus-driven differentiation of marrow stromal cells in 3D scaffolds that is independent of myosin-based cytoskeletal tension. Biomaterials 2011;32:2256–2264.

34. Pei YZ, Liu X, Liu SS, Lu Q, Liu J, Kaplan DL, et al. A mild process to design silk scaffolds with reduced beta-sheet structure and various topographies at the nanometer scale. Acta Biomaterialia 2015;13:168–176.